

Cite this: *Environ. Sci.: Nano*, 2021, 8, 2464

Understanding the toxicity mechanism of CuO nanoparticles: the intracellular view of exposed earthworm cells†

Natividad Isabel Navarro Pacheco,^{ab} Radka Roubalova,^a Jiri Dvorak,^a Oldrich Benada,^a Dominik Pinkas,^c Olga Kofronova,^a Jaroslav Semerad,^{ae} Martin Pivokonsky,^d Tomas Cajthaml,^{ae} Martin Bilej^a and Petra Prochazkova^{ae*}

Copper oxide nanoparticles (CuO NPs) are widely used in industry. Once released, they can enter the soil system and endanger organisms living in this environment. Therefore, monitoring the NP impact on soil organisms and identification of suitable biomarkers associated with NP pollution are required. In this study, immune effector cells of the earthworm *Eisenia andrei*, amoebocytes, were exposed to environmentally relevant sublethal concentrations of CuO NPs (1, 10, and 100 $\mu\text{g mL}^{-1}$ of Cu) and their impact on the cellular and subcellular levels, as well as on the mRNA levels of molecules involved in the defense reactions, was assessed *in vitro*. CuO NPs decreased the viability of both amoebocyte subpopulations by 40% at the highest concentration tested (100 $\mu\text{g mL}^{-1}$ of Cu). Further, CuO NPs caused significant attenuation of the phagocytic function of hyaline amoebocytes after 6 and 24 hours of exposure, by 37 and 25%, respectively. The concentration of the lipid peroxidation subproduct, malondialdehyde, was 10 times elevated in cells exposed to CuO NPs (100 $\mu\text{g mL}^{-1}$ of Cu) after 6 hours of exposure. We hypothesize that malondialdehyde may induce DNA breaks, cell cycle arrest, and subsequent cell death. Electron microscopy showed the interaction between CuO NPs and immune effector cells, amoebocytes. Moreover, aggregates of CuO NPs were shown to be engulfed and located in the cytoplasm of these cells. However, data from all experiments indicate that the observed effects of CuO NPs on earthworm coelomocytes were caused mainly by the dissolved Cu^{2+} ions derived from nanoparticles (NPs). The determination of effective parameters such as oxidative stress, immune reactivity, and genotoxicity would provide valuable comprehension and data for environmental assessment of NP impact on soil organisms.

Received 22nd January 2021,
Accepted 25th June 2021

DOI: 10.1039/d1en00080b

rs.li/es-nano

Environmental significance

The increasing production of copper oxide nanoparticles (CuO NPs) leads to the larger availability of released NPs in the soil system. Earthworms as soil ecosystem engineers and the most important detritivores in soils are in the base of the food chain. In order to predict the immunological risk of nanomaterials on earthworms, we investigated the effects of engineered CuO NPs on earthworm innate immune responses. The proposed study shows that earthworm cells interact with CuO NPs and engulf them and that this interaction leads to the modified cell physiology. CuO NP immunosafety depends primarily on the NP concentration that affects the cells and on the effect of dissolved Cu^{2+} ions derived from nanoparticles.

^a Institute of Microbiology of the Czech Academy of Sciences, Videnska 1083, 142 00 Prague 4, Czech Republic. E-mail: kohler@biomed.cas.cz

^b First Faculty of Medicine, Charles University, Prague, Czech Republic

^c Institute of Molecular Genetics of the Czech Academy of Sciences, Microscopy Centre, Electron Microscopy Core Facility, Videnska 1083, 142 20 Prague 4, Czech Republic

^d Institute of Hydrodynamics of the Czech Academy of Sciences, Pod Patankou 30/5, 166 12, Prague 6, Czech Republic

^e Institute for Environmental Studies, Faculty of Science, Charles University, Benatska 2, 128 01 Prague 2, Czech Republic

† Electronic supplementary information (ESI) available. See DOI: 10.1039/d1en00080b

1. Introduction

Nanomaterials (NMs) and nanoparticles (NPs) are produced worldwide with an increased production volume year by year. It is expected to reach 174 billion dollars by 2025 at the global market, which will be around 18% of the annual growth rate.¹ As a consequence of this growth, NPs can be released indirectly into the environment. Recent studies have shown that the soil system is predominately the greatest recipient of NPs coming from water, wastewater treatment sludge, and landfills.² Therefore, the exploration of the

effects of NPs on the environment and soil organisms is extremely important for a proper ecological risk assessment.

Among the manufactured NPs, copper oxide nanoparticles (CuO NPs) are mainly used in the production of gas sensors, semiconductors, thin films for solar cells, catalysts, ceramic pigments, and biocides for agriculture. By its worldwide production and use, CuO NPs can be accidentally released at different stages of their life cycle and reach the environment. Moreover, CuO NPs and Cu-based NPs are common nanopesticides that could be found easily in the terrestrial ecosystem; thus, soil organisms and their microbiome could be affected.³

Among the soil organisms, earthworms represent very important soil invertebrates that participate in nutrient cycling in terrestrial ecosystems. Due to their permanent direct contact with soil and soil microbiota, earthworms have developed strong defense reactions protecting them against pathogens. However, soil pollutants can also affect them.⁴ Earthworms can bioaccumulate organic compounds,^{5,6} metals,⁷ and NPs.^{8,9} Two earthworm species, *Eisenia andrei* and *E. fetida*, are used as models for monitoring ecotoxicity (OECD, ISO protocols).

The most common pathway through which metal pollutants enter the earthworm body is the skin.^{10,11} Subsequently, metal pollutants enter the coelomic cavity filled with coelomic fluid containing free-floating cells, coelomocytes. These coelomocytes can be classified into three populations: free chloragogen cells (eleocytes) with mainly nutritive function, and granular and hyaline amoebocytes possessing immune function.¹² Several studies have described the use of flow cytometry as a useful tool to differentiate eleocyte and amoebocyte populations. The separation of cell populations allows the evaluation of cellular responses to various factors, such as pathogens and pollutants.^{13–16} Amoebocytes are immune effector cells participating in both cellular immune reactions (phagocytosis or encapsulation) and humoral immune responses. NPs can be internalized by amoebocytes *via* endocytosis/phagocytosis, suggesting that phagocytic cells could be more affected by NPs than other cell types.^{17,18}

Depending on the type of NPs and their physico-chemical characteristics, diverse effects could be observed in the earthworm. It has been reported that CeO₂ and SnO₂ NPs don't affect earthworm reproduction and growth and are scarcely accumulated in earthworms.¹⁹ The toxic effects of ZnO NPs on earthworms were caused by oxidative stress in a concentration-dependent manner.^{20,21} Even though mortality or reproduction is not affected by NPs (ZnO NPs, Ag NPs, TiO₂ NPs), oxidative stress seems to be the most probable cause by which earthworms could be damaged.²²

Ag NPs have been described to alter the expression of genes involved in immune signaling and oxidative stress, while TiO₂ NPs have not been able to activate the antioxidant system even though ROS have been produced.^{15,17,23} The toxicity response occurred with coated CuO NPs in contrast to its equivalent uncoated CuO NPs.²⁴ ZnO NPs were taken

up by coelomocytes, leading to molecular damage and cell death.¹⁸ Recently, immunotoxicity has brought up a new perspective to understand the toxicity mechanism at the level of sublethal effects. CuO NPs have been reported to inactivate antioxidative enzymes in common Indian *M. posthuma* earthworms.²⁵ The inactivation of the antioxidative system can compromise the earthworm's innate immune system and it can adversely affect the defense reactions.

In this context, our study is focused on the toxicity mechanism during *in vitro* exposure of coelomocytes of earthworm *Eisenia andrei* to sublethal doses of CuO NPs (1, 10, and 100 $\mu\text{g mL}^{-1}$ of Cu). CuO NP characterization was performed to provide their size distribution and shape. Scanning and transmission electron microscopy provided images of NPs distributed in the cell. Furthermore, oxidative stress, phagocytic activity, cell death program and mRNA levels were analyzed in cells exposed to CuO NPs and CuSO₄ after 2, 6 and 24 h. These analyses could be used for future ecological risk assessments in soil ecosystems.

2. Materials and methods

2.1 Sample collection

Experiments were performed using adult *Eisenia andrei* earthworms from our laboratory compost breeding. Earthworm guts were allowed to empty for 48 hours at room temperature on moistened filter paper prior to cell harvesting. Earthworms were depleted of coelomocytes in 15 mL Falcon tubes with an extrusion buffer (2 mL per earthworm; 6.8 mM EDTA, 50.4 mM guaiacol glyceryl ether in diluted PBS (3:2), 176 mOsm, pH 7.3) for 2 min. The harvested cells were cleaned by two cycles of centrifugation and washing ($150 \times g$, 4 °C, 10 min) with PBS (3:2). Cells were counted to obtain 2×10^5 cells per well for the assessment of apoptosis and phagocytosis. For lipid peroxidation assessment, TEM, and SEM, 10^6 cells per well were used. Then, cells were exposed to freshly prepared dispersions of CuO NPs (1, 10 and 100 $\mu\text{g mL}^{-1}$) and CuSO₄ (1, 10 and 100 $\mu\text{g mL}^{-1}$) representing the same nominal concentration of Cu during the exposure (*i.e.* 1, 10, and 100 $\mu\text{g mL}^{-1}$ of Cu). For the dispersion of NPs and cell cultivation, we prepared the cultivation medium with osmolality adjusted to the growth medium based on RPMI-1640 containing L-glutamine (BioWhitaker®), and supplemented with 100 mM HEPES (pH 7.0–7.6, Sigma-Aldrich), 20 mM Na-pyruvate (Sigma-Aldrich), 100 mg mL⁻¹ gentamicin, antibiotic-antimycotic solution (Sigma Aldrich), and 2.5% heat-inactivated fetal bovine serum (FBS).¹⁴ Then, the prepared RPMI 1640-medium was diluted with autoclaved MilliQ-water to 60% (v/v) called R-RPMI 1640.²⁶ All analyses were performed in the dark at 20 °C for 2, 6, and 24 h.

2.2 Characterization of nanoparticles (NPs)

Nanoparticles (NPs) used in the present study were purchased from the Promethean company (Promethean Particles LTD., Nottingham, United Kingdom). Primary size

and shape were analyzed by transmission electron microscopy (TEM) (Fig. S1†). NPs were thoroughly characterized for their physico-chemical properties and behavior in the exposure media (MilliQ water and R-RPMI 1640 cultivation medium). The data obtained from all measurements are summarized in Table S1.† For our experiments, CuO NPs were incubated in R-RPMI 1640 cultivation medium for 2, 6, and 24 h at three different concentrations (1, 10, and 100 $\mu\text{g mL}^{-1}$ of Cu). An inductively coupled plasma optical emission spectrophotometer (ICP-OES, 5110 Series, Agilent Technologies, USA) was used to determine the dissolved copper concentrations in the cultivation medium. Samples were centrifuged four times (18 400 $\times g$, 4 $^{\circ}\text{C}$, 10 min) for settling down the NPs. The supernatants were analyzed by ICP-OES to determine the Cu concentration. The Cu concentration was determined in parallel also for the three concentrations of CuSO_4 (1, 10, and 100 $\mu\text{g mL}^{-1}$ of Cu). Metal detection and quantification in the samples were carried out in triplicate, and instrumental errors were less than 3%. The Z-potential and hydrodynamic diameter of the nanoparticles (MADLS) were determined using a Zetasizer Ultra (Malvern Panalytical). To avoid positive signals from the cultivation medium, a negative control represented by the cultivation medium without NPs was included in all assays.

2.3 Scanning and transmission electron microscopy (SEM and TEM)

2.3.1 Cell fixation. After cell exposure (2, 6, and 24 h) to CuO NPs, cells were collected into 48 well plates (1×10^6 per well). The cell viability was checked by flow cytometry and propidium iodide staining. Cells were mixed with a 2.5% fixation solution (1 mL $5\times$ PBS (3:2); 1 mL glutaraldehyde (25%), and 3 mL distilled water) in a 1:1 (v:v) ratio. Fixed cells were moved gently for 15 min and kept overnight at 4 $^{\circ}\text{C}$.

2.3.2 SEM samples. For SEM sample preparation, fixed cells were washed with PBS (3:2) buffer three times at room temperature for 20 min, spun down at 150 $\times g$, and then allowed to adhere onto poly-L-lysine coated coverslips in the refrigerator overnight. The coverslips with attached cells were washed with ddH₂O and fixed with 1% OsO₄ for one hour at room temperature. The coverslips were washed three times for 20 min each, dehydrated through an alcohol series (25, 50, 75, 90, 96, and 100%), and were critical point dried from liquid CO₂ in a K850 critical point dryer (Quorum Technologies Ltd, Ringmer, UK). The dried coverslips were sputter-coated using a high-resolution turbo-pumped sputter coater Q150T (Quorum Technologies Ltd, Ringmer, UK) with 3 nm of platinum. The final samples were examined in a FEI Nova NanoSEM scanning electron microscope (FEI, Brno, Czech Republic) at 5 kV using CBS and TLD detectors. An electron beam deceleration²⁷ mode of the Nova NanoSEM scanning electron microscope performed at a StageBias of 883.845 V and accelerating voltage of 5 kV was used for high-resolution imaging. The EDS microanalysis was performed at 15 kV using an Ametek® EDAX Octane Plus SDD

detector and TEAM™ EDS analysis systems (AMETEK, B. V.; Tilburg, The Netherlands).

2.3.3 TEM samples. For TEM sample preparation, the cells under gentle agitation were fixed as described above. After exhaustive washing, cells were post-fixed with 1% OsO₄ in PBS (3:2) overnight at 4 $^{\circ}\text{C}$. Cells were washed three times in PBS buffer at 4 $^{\circ}\text{C}$, and then with ddH₂O. After washing, the cell suspension was warmed up to room temperature and embedded into 4% low-melting agarose. Solidified agarose was cut into small cubes and the cubes were dehydrated in an alcohol series. Finally, the agarose cubes were embedded into an epoxy resin (EMBed-812 Embedding kit; Electron Microscopy Sciences). Ultrathin sections were contrasted using uranyl acetate and lead citrate²⁸ and examined in a Philips CM100 electron microscope (Eindhoven, The Netherlands, Thermo Fisher Scientific). Digital images were recorded with a Veleta slow-scan camera (EMSIS GmbH, Germany), and processed using the iTEM software package.

Transmission electron microscopy of CuO NPs was performed by the application of the nanoparticle suspension (5 μL) onto glow-discharge activated²⁹ 400 mesh copper grids coated with an ultrathin carbon support film. The nanoparticles were allowed to sediment for one minute. The remaining solution on the grids was blotted with filter paper and the grids were air-dried. The grids were examined in a Philips CM100 electron microscope equipped with a Veleta CCD slow-scan camera (EMSIS GmbH, Muenster, Germany). TEM images were processed in the iTEM software (EMSIS GmbH, Muenster, Germany) using standard modules (shading correction, digital contrast enhancement). CuO nanoparticle size was estimated by manual measurement³⁰ and also by the particle analysis module of the iTEM software.

2.3.4 STEM and X-ray microanalysis. The ultrathin sections were mounted onto Ti-grids (SPI Supplies, Structure Probe, Inc. West Chester, PA, USA) to eliminate spurious X-rays from the Cu-grids. The subsequent grid processing was then the same as described for TEM samples on Cu-grids. STEM images and EDS spectra were recorded on the JEOL F200 instrument with cold FEG operated at 200 kV and equipped with a HAADF detector and JED-2300 X-ray spectrometer with a windowless SDD detector (JEOL Ltd., Akishima, Tokyo, Japan). Point spectra were acquired with a total live time of 60 seconds, and maps with a resolution of 256 \times 256 points were recorded with a total live time of 600 seconds at electron beam intensity set so that the X-ray detector accumulates at least 1000 cps on the empty resin.

2.3.5 Electron microscopy data processing. Proprietary software of electron microscopes and X-rays analyzers was used for primary data processing. For publishing, the original 16bit greyscale images were exported to 8bit grayscale TIFFs. The spectra from the JED-2300 X-ray spectrometer were exported into industry-standard EMSA format for further processing. All presented spectra were processed in the NIST DTSA-II software (Lorentz revision).³¹ The image plates (Fig. 2 and 3) were produced in the open source Inkscape (<https://inkscape.org>).

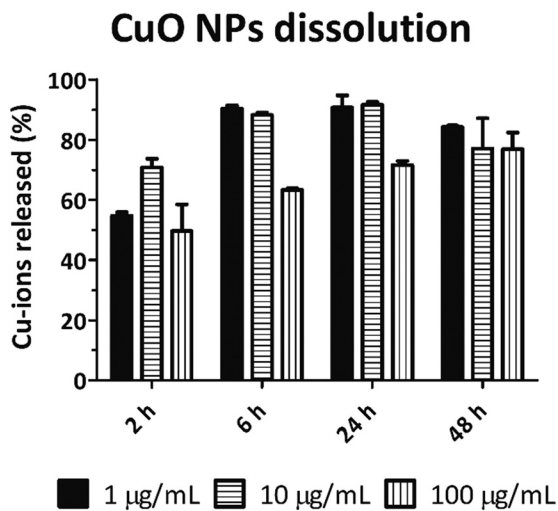


Fig. 1 CuO NP dissolution in R-RPMI 1640 cultivation medium. Different concentrations of CuO NPs (1, 10, and 100 $\mu\text{g mL}^{-1}$ of Cu in the form of CuO NPs) were added into R-RPMI 1640 cultivation medium. The Cu-ions released in the cultivation medium upon 2, 6, 24 and 48 h of exposure time were quantified by ICP-OES. Values are shown as the mean \pm SD of three measurements with three replicates.

2.4 Flow cytometry

Apoptosis and phagocytosis were measured using a laser scanning flow cytometer (LSR II; BD Biosciences), and data were analyzed by FlowJo software (9.9.4 version, BD Biosciences, San Jose, CA, USA). Three different subsets of coelomocytes were detected (eleocytes, hyaline and granular amoebocytes). Each subset was related to cell size (FSC) and cell inner complexity/granularity (SSC). Propidium iodide (PI; 1 $\mu\text{g mL}^{-1}$; Sigma-Aldrich, Steinheim, Germany) was added to the cell sample in each experiment before the measurement.

Each experiment also included medium analysis to avoid interferences coming from the cultivation medium or the NPs.

2.4.1 Apoptosis. After the different cell incubation exposure times (2, 6, and 24 h) with CuO NPs or CuSO₄ (1, 10, and 100 $\mu\text{g mL}^{-1}$ of Cu), cell suspensions were washed twice (150 $\times g$, 4 $^{\circ}\text{C}$, 10 min) with Annexin V binding buffer. According to the manufacturer, a stock solution of Alexa-Fluor 647-Annexin V was prepared (Thermo Fisher Scientific, Eugene, OR, USA). Then, 15 μL from the stock solution was added over 15 min in darkness. Subsequently, PI (1 $\mu\text{g mL}^{-1}$) in Annexin V binding buffer was added, and the cells were analyzed by flow cytometry. The apoptosis/necrosis % represented the apoptotic/necrotic cell number out of each subpopulation.

2.4.2 Phagocytosis. After coelomocyte cultivation with CuO NPs or CuSO₄ for 2, 6, 24 h, latex beads (Fluoresbrite®Y Microspheres 1 μm ; Polyscience Inc., Warrington, PA, USA) were added to the suspensions in a 1 : 100 (cells : beads) ratio, and the cells were cocultivated for 18 h at 17 $^{\circ}\text{C}$ in darkness. Then, the cell suspensions were washed twice with PBS (3 : 2) buffer and centrifuged (150 $\times g$, 4 $^{\circ}\text{C}$, 10 min) to exclude free beads. PI (1 $\mu\text{g mL}^{-1}$) was added and phagocytic activity as well as cell viability was measured by flow cytometer. The presence of phagocytosed beads was analyzed by confocal microscopy. The % phagocytic activity was determined by the % of alive cells, which were able to engulf at least one bead out of each subpopulation.

2.5 Lipid peroxidation

The concentration of malondialdehyde (MDA) produced was determined by high-performance liquid chromatography with

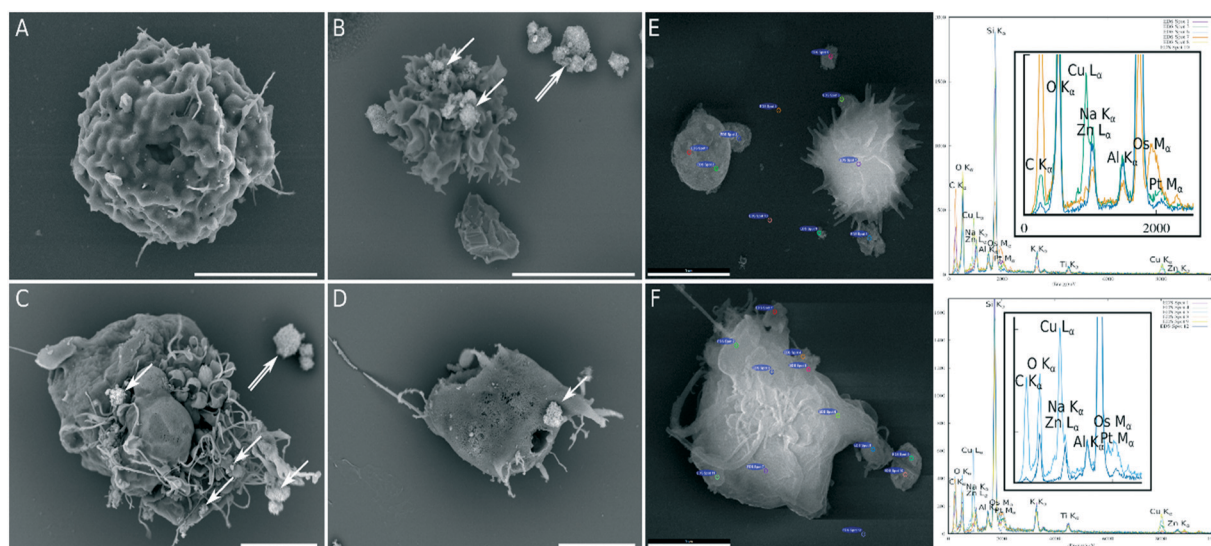


Fig. 2 Scanning electron microscopy images of CuO NPs. A) Non-treated coelomocytes in R-RPMI 1640 medium after 2 h exposure, B–D) coelomocytes incubated with 100 $\mu\text{g mL}^{-1}$ of Cu in the form of CuO NPs for 2, 6, and 24 h. E) EDS analysis of coelomocytes, F) EDS analysis of coelomocytes with identified CuO NPs on their surface. The scale bars represent 10 μm (A and B) and 5 μm (C–F). The white arrows indicate the location of CuO NPs on the coelomocyte surface.

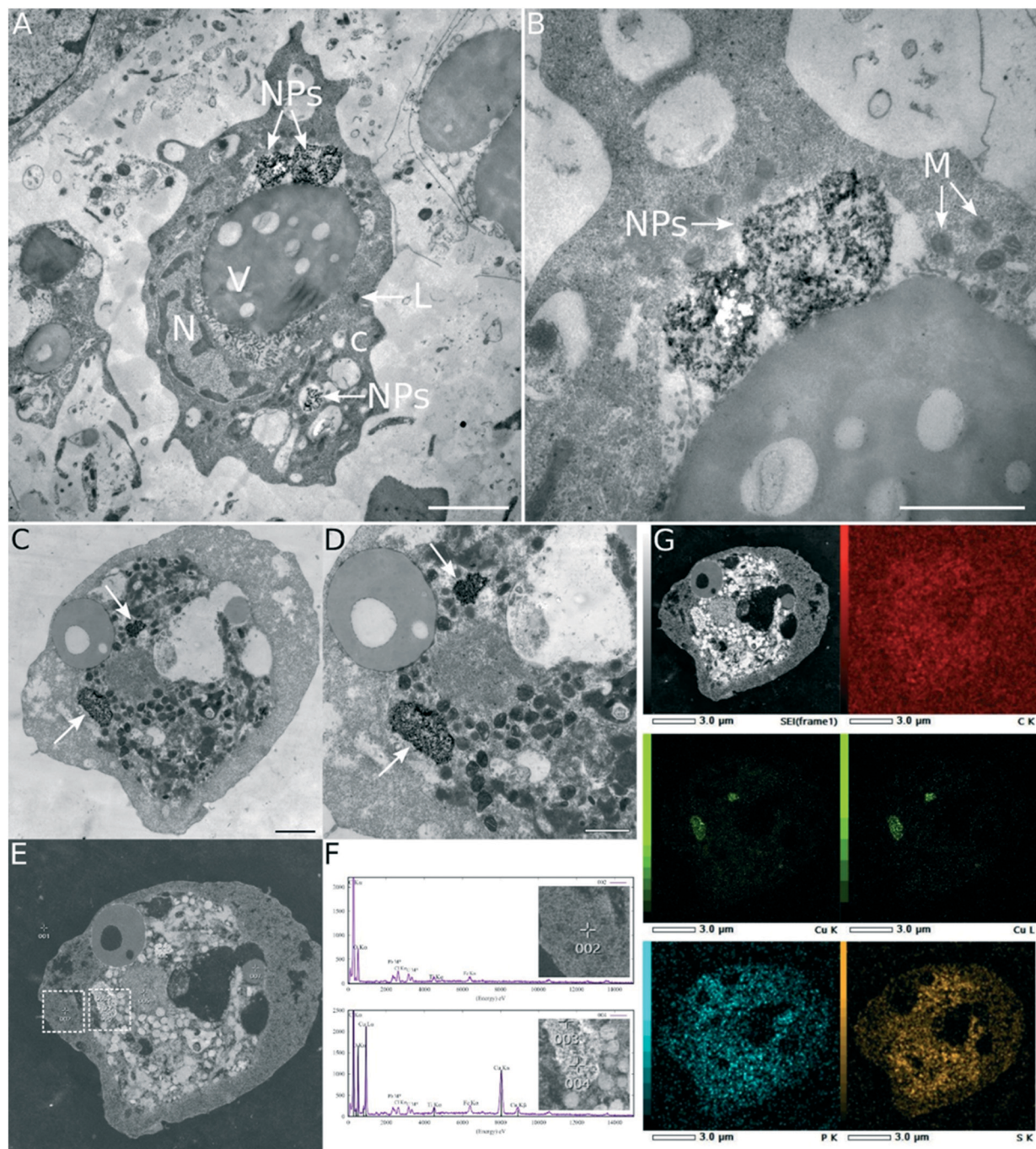


Fig. 3 Transmission electron microscopy and STEM/EDS microanalysis of coelomocytes incubated with CuO NPs. Ultrathin sections of coelomocytes incubated with $100 \mu\text{g mL}^{-1}$ of Cu in the form of CuO NPs for two hours mounted onto a Cu-grid (A and B). C and D: Ultrathin sections of the cells treated with $100 \mu\text{g mL}^{-1}$ of CuO NPs for 6 hours mounted onto a Ti-grid. The arrows point to the CuO-NP clusters in the cytoplasm, Philips CM100 electron microscope. E: STEM HAADF image of the same section as in panels C and D; JEOL F200 electron microscope. The dashed squares marked the areas from the spectra in D originate. F: An example of two characteristic spectra taken from the cytoplasm near the CuO NP cluster (upper) and directly from the CuO NP cluster (lower). The main Cu $K\alpha$ (8.048 keV) and Cu $L\alpha$ (0.929 keV) peaks are clearly shown in the lower spectrum, confirming copper's presence in the electron-dense aggregates in the cytoplasm unequivocally. The other detected elements originate from sample processing (Pb and U from contrasting, according to Reynolds, 1963) or from the supporting grid (Ti) or microscope pole pieces (Fe). Carbon and oxygen are typical for biological matter. Six panels in section G represent selected EDS maps. The Cu maps ($K\alpha$ and $L\alpha$) confirmed the copper's localization in the electron-dense clusters marked with arrows in panels C and D. All spectra and elemental maps were recorded in a JEOL F200 using a JED-2300 X-ray spectrometer with a windowless SDD detector. The scale bars represent $2 \mu\text{m}$ in A and C panels and $1 \mu\text{m}$ in B and D panels. M – mitochondria, N – cell nucleus, L – lysosome, V – vacuoles, NPs – nanoparticles, and C – cytoplasm.

fluorescence detection (HPLC/FLD) using derivatized MDA-TBA2.³² After the incubation times (2, 6, and 24 h) with CuO NPs or CuSO₄ (10 and 100 µg mL⁻¹ of Cu), cells were collected and the MDA concentration was measured.

2.6 Comet assay

The comet assay procedure was based on previously described assays^{33,34} with slight modifications. Glass slides were precoated with 1% agarose. The comet assay was carried out by exposing the coelomocytes to different CuO NP and CuSO₄ concentrations (1, 10, and 100 µg mL⁻¹ of Cu) for various exposure times (2, 6, and 24 h). Subsequently, 1.5×10^4 cells were mixed with 2% 2-hydroxyethyl agarose (LMA; Sigma-Aldrich, Steinheim, Germany) at 37 °C, put on the precoated slide, and kept for 10 min at 4 °C. Another LMA layer was added to split the cells and cover all pores for better microscopic analysis (10 min, 4 °C). Slides were then introduced into fresh lysis buffer for 2 h (2.5 M NaCl, 10 mM Tris-HCl, 100 mM EDTA, 1% Triton-100X; pH 10). Then, slides were incubated in unwinding buffer (0.03 M NaOH, 2 mM EDTA; pH 12.7) three times for 20 min each. Gel electrophoresis was conducted at 24 V, 300 mA for 25 min. Glass slides were rinsed 3 times in neutralizing buffer (0.4 M Tris; pH 7.5) for 5 min at room temperature and stained with PI (3 µg mL⁻¹) for 20 min in darkness. Excess stain was washed in distilled water for 5 min. Glass slides were then kept for a short period in humidified chambers. One hundred cells per replicate of each treatment and time interval were analyzed using the LUCIA Comet Assay software, and the mean of DNA content in 100 comet tails (%) was calculated as a parameter of DNA damage.

2.7 RNA isolation, cDNA synthesis, qPCR

RNA was isolated from coelomocytes using the RNAqueous@-Micro Kit (Invitrogen, Vilnius, Lithuania). 500 ng of DNase I treated total RNA was reverse-transcribed using the Oligo(dT)12–18 primer and Superscript IV Reverse Transcriptase (Life Technologies, Carlsbad, CA, USA), and subsequently used in a PCR reaction. Non-RT controls were run in parallel to prove the elimination of gDNA contamination.

Quantitative PCR (CFX96 Touch™, Bio-Rad) was performed to determine the changes in the mRNA levels of metallothionein, phytochelatin, Mn-SOD (superoxide dismutase), CuZn-SOD, catalase, EMAP II (endothelial monocyte-activating polypeptide II), fetidin/lysenin, lumbricin, MEK kinase 1, and protein kinase C 1 (primer sequences are shown in Table S2†). Each reaction was performed in 25 µl containing 4 µl of cDNA sample (dilution 1/10 except for 1/5 dilution for SODs). The cycling parameters were as follows: 4 min at 94 °C, 35 cycles of 10 s at 94 °C, 25 s at 60 °C (at 58 °C for MEK kinase I, protein kinase C 1, and catalase), 35 s at 72 °C, and a final extension for 7 min at 72 °C. The specificity and efficacy of primer pairs were confirmed by melt curve analysis of resulting PCR products. Gene expression changes were calculated according to the 2^{-ΔΔCT} (Livak) method. Two

reference genes (RPL13, RPL17) were selected as internal controls for the normalization of the other gene expression. Non-template controls were included in each experiment. The fold change in the mRNA level was related to the change in the settled controls. The results were expressed as the mean ± SEM of the values. Evidence of significant changes was evaluated using two-way ANOVA with the Bonferroni post-test in the GraphPad Prism software.

2.8 Statistical analyses

All parameters were measured in triplicate. Data were expressed as mean ± SEM of the values obtained in three different independent experiments. Two-way analysis of variance (ANOVA) with the Bonferroni post-test was performed using GraphPad Prism software (8.3.1 version, San Diego, CA, USA) to evaluate the significance of the data. Differences were considered significant when $p < 0.05$, $p < 0.01$ and $p < 0.001$.

3. Results

3.1 Characterization of nanoparticles

The primary size and shape of CuO NPs were analyzed by TEM (Fig. S1†). Our observations showed that primary particle sizes ranged from 5 to 15 nm, while the manufacturer (Promethean) stated 15–50 nm (Fig. S1†). The rod shape of CuO NPs announced by Promethean was in line with our results.

The results obtained from the ICP-OES analysis showed that NPs were not stable along time and in lower concentrations (1, 10 µg mL⁻¹ of Cu), as the release of Cu²⁺ ions was detected (Fig. 1). Concerning 100 µg mL⁻¹ of Cu in the form of CuO NPs, the solubility was proved over the different exposure times, with slower ion release compared to 1 and 10 µg mL⁻¹ of Cu in the form of CuO NPs. The same analysis was performed with CuSO₄ samples used as a control, which showed that CuSO₄ is completely dissolved after 2 h of exposure for all dilutions (1, 10, and 100 µg mL⁻¹ of Cu; data not shown). Physico-chemical properties of NPs are summarized in Table S1.† The data obtained were compared between MilliQ water and R-RPMI 1640 cultivation medium for better comprehension of the NP interaction with the medium. UV/vis values were obtained by UV/vis spectrophotometry for 100 µg mL⁻¹ of Cu in the form of CuO NPs (Table S1†). All techniques (ICP-OES, TEM, MADLS, Z-potential, and UV/vis) used coincidentally showed that CuO NPs are unstable and have a tendency to aggregate. The remarkable changes were found in R-RPMI 1640 medium used for the analysis, suggesting its effect on the CuO NP dispersion (Table S1†). Further, it was observed that 100 µg mL⁻¹ of Cu in the form of CuO NPs exerted much slower dissolution, most probably due to the aggregation of nanoparticles creating clusters of 350 nm in size, while the primary NP size ranged between 5 and 15 nm.

3.2 Electron microscopy

Transmission and scanning electron microscopy highlighted the interaction of CuO NPs with immune cells, and showed the NP distribution on and in the cells (Fig. 2 and 3). Energy-dispersive X-ray spectroscopy (EDS) in SEM showed that the objects observed on the cell surface were CuO NPs (Fig. 2E and F). The elemental composition of various spots was assessed.

Three spots representing different types of matter were analyzed; spot 3 – CuO NPs, spot 7 – coelomocyte, spot 10 – background-coated coverslip. Uniquely in spot 3, we observed a Cu peak, while there was no peak corresponding to Cu in spots 7 and 10 (Fig. 2E). Fig. 2F shows a coelomocyte with identified CuO NPs on its surface. The analysis of spot 5 revealed a high Cu ($K\alpha$, 8.048 keV) peak and carbon ($K\alpha$ 0.277 keV) peak coming from the organic material of the cell, which indicates that the NPs are over the cell surface. On the other hand, we could determine that there is no copper signal coming from spot 12 (background-covered coverslip).

Notably, we observed that the quantity of NPs decreased along the exposure times (2, 6, and 24 h) when 10 and 100 $\mu\text{g mL}^{-1}$ of Cu concentrations were used. As explained above, at the least concentration (1 $\mu\text{g mL}^{-1}$ of Cu), no CuO NPs were detected in the medium because they had dissolved. At the 100 $\mu\text{g mL}^{-1}$ of Cu concentration, CuO NPs aggregated and their clusters were found around the cell surface (Fig. 2B, C, and D – white arrows; Fig. 2A shows a non-treated cell). TEM analysis revealed the intracellular location of CuO NPs (Fig. 3). Aggregates of CuO NPs (100 $\mu\text{g mL}^{-1}$ of

Cu) were engulfed and located in the cytoplasm; however, they were not in the nucleus (N) or mitochondria (M) (Fig. 3A–D). Finally, the STEM/EDS-microanalysis unambiguously confirmed the presence of copper in those aggregates (Fig. 3E–G).

3.3 Analysis of coelomocyte populations by flow cytometry

Flow cytometry was used for several cell analysis investigations (apoptosis, necrosis, and phagocytosis). We succeeded in differentiation of three different coelomocyte populations. Two subsets of amoebocytes (hyaline and granular) were detected based on their size and granularity (Fig. S2–S4†). The eleocyte population was not included in subsequent analyses due to its high autofluorescence, which would lead to false-positive results.

3.3.1 Analysis of apoptosis. The percentages of cells that underwent early and late apoptosis and necrosis, and the viability of both granular and hyaline amoebocytes were detected (Fig. 4 and 5). The cell viability (the percentage of alive cells in each subpopulation) ranged between 70 and 85% after 2 h of cell incubation with 100 $\mu\text{g mL}^{-1}$ of Cu in the form of CuSO_4 and CuO NPs. After 24 h of incubation, the viability decreased to 30–50% when 100 $\mu\text{g mL}^{-1}$ of Cu in the form of CuSO_4 and CuO NPs were used (Fig. 4 and 5). The viability was approximately the same (65–76%) at the time of exposure (2, 6, and 24 h) for the non-treated cells (Fig. 4 and 5).

Both coelomocyte populations (HA and GA) showed a similar shift between different stages of early and late apoptosis/necrosis upon interaction with CuO NPs during

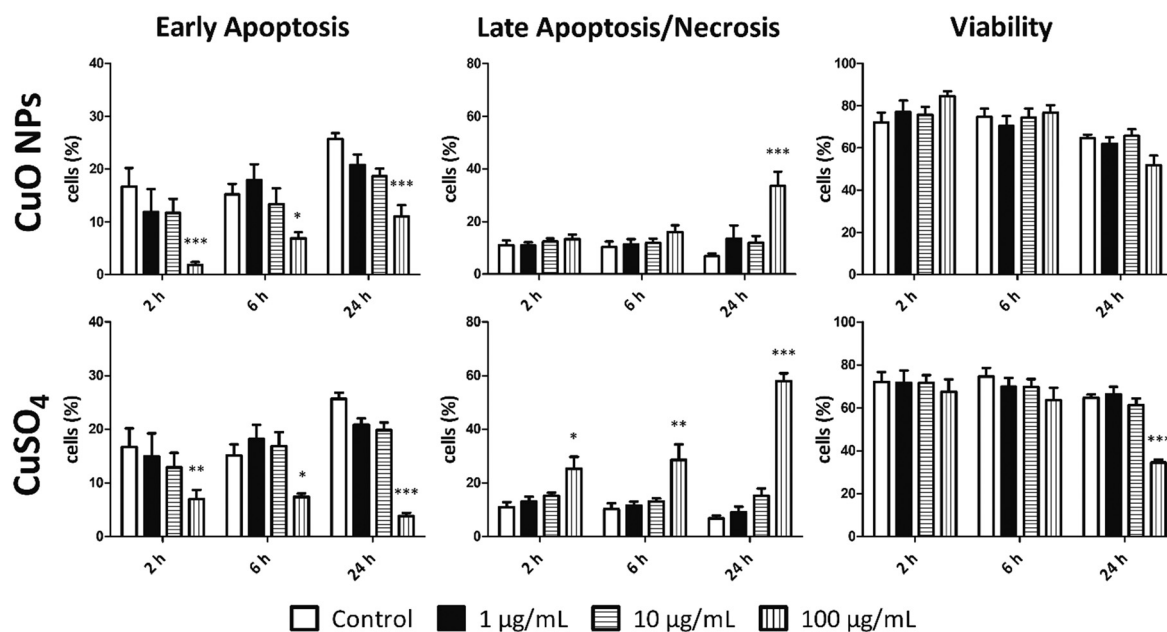


Fig. 4 Early apoptosis, late apoptosis/necrosis and viability of hyaline amoebocytes (HA). Early apoptosis, late apoptosis/necrosis of HA of non-treated cells, cells exposed to CuO NPs and CuSO_4 at 1, 10, and 100 $\mu\text{g mL}^{-1}$ of Cu and for 2, 6, and 24 h. The results are shown as mean (%) \pm SEM of three independent experiments with 3 replicates in each. *** $p < 0.001$, ** $p < 0.01$ and * $p < 0.05$ according to two-way ANOVA and Bonferroni post-test.

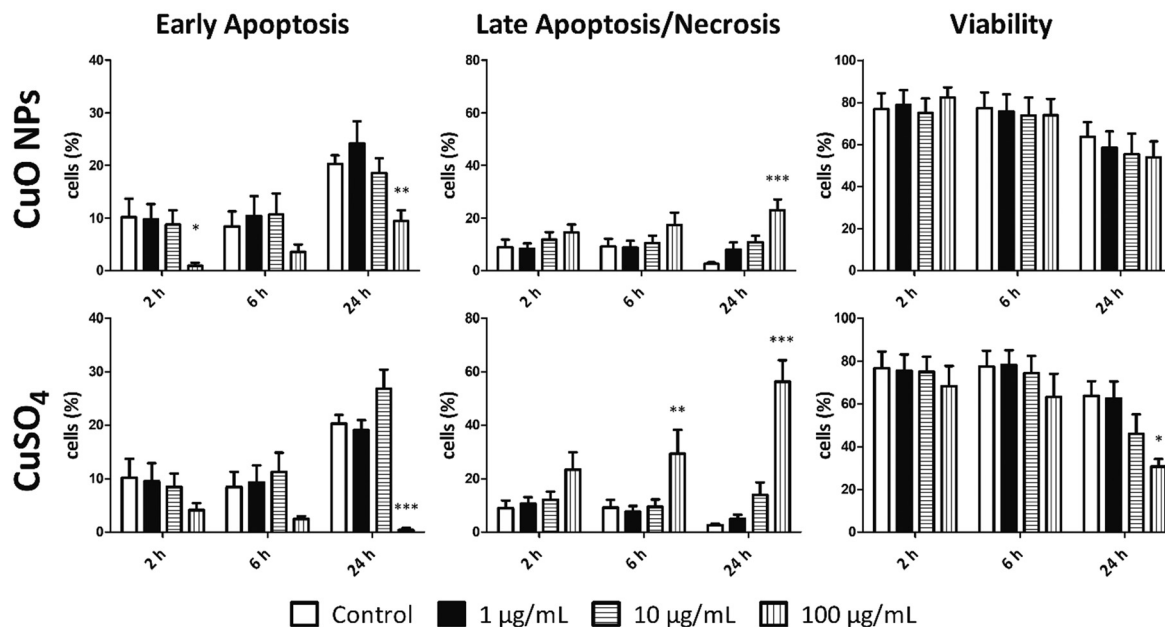


Fig. 5 Early apoptosis, late apoptosis/ necrosis, and viability of granular amoebocytes (GA). Early apoptosis, late apoptosis/necrosis of GA of non-treated cells, cells exposed to CuO NPs and CuSO₄ at 1, 10, and 100 µg mL⁻¹ of Cu and for 2, 6, and 24 h. The results are shown as mean (%) ± SEM of three independent experiments with 3 replicates in each. ****p* < 0.001, ***p* < 0.01 and **p* < 0.05 according to two-way ANOVA and Bonferroni post-test.

the entire incubation time (Fig. 4 and 5). However, only the highest concentration of Cu NPs elicited a significant decrease of cell number in early apoptosis and an increase of late apoptotic/necrotic cell number. Similarly, an increasing tendency toward late apoptosis/necrosis and a decreasing tendency to early apoptosis were detected along the incubation times (2, 6, and 24 h) in both subpopulations exposed to the highest concentration of CuSO₄ (Fig. 4 and 5). The highest portion of late apoptotic/necrotic cells was detected after 24 hours of incubation with both forms of Cu. Cu in the ionic form (CuSO₄) induced a greater rate of apoptosis compared to CuO NPs. That is reflected in the lower viability of cells incubated with CuSO₄ at the end of incubation (24 h; Fig. 4 and 5).

3.3.2 Phagocytic activity. To assess the impact of CuO NPs on cellular immune reactions, the phagocytic activity of the viable amoebocytes was determined. Approximately 55–60% of hyaline amoebocytes and 47–50% of granular amoebocytes are phagocytic during 6 h of cultivation (Fig. 6). Cell treatment with the greatest concentration of CuO NPs led to the decrease of the phagocytic activity along the exposure time. This tendency was seen in both subsets of amoebocytes; however, significant changes were seen only in the hyaline amoebocyte population.

Surprisingly, granular amoebocytes are less sensitive than hyaline amoebocytes to CuO NP treatment (Fig. 6A). In the hyaline amoebocyte subset, the phagocytic activity decreased significantly at 100 µg mL⁻¹ of Cu in the form of CuO NPs after 6 and 24 h of incubation, by 37 and 25%, respectively.

The same CuSO₄ concentration exerted a similar tendency to CuO NPs for both amoebocyte subsets (Fig. 6B). The observed phagocytic inhibition could be related to the great cell number in necrosis (Fig. 6), which lost their ability to

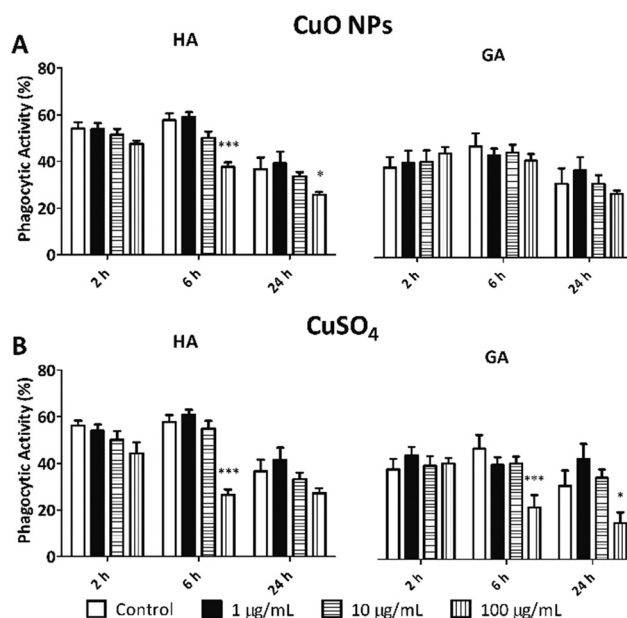


Fig. 6 Phagocytic activity of hyaline (HA) and granular amoebocytes (GA). Phagocytic activity was measured for hyaline (HA) and granular amoebocytes (GA) after treatment with 1, 10, and 100 µg mL⁻¹ of Cu in the form of A) CuO NPs and B) CuSO₄ for 2, 6, and 24 h. Data are expressed as a percentage of the phagocytic activity and mean ± SEM of three experiments with three replicates. ****p* < 0.001, ***p* < 0.05 according to two-way ANOVA and Bonferroni post-test.

phagocytose. Interestingly, CuSO_4 induced even greater phagocytic inhibition (50%) in both amoebocyte subpopulations than CuO NPs after 6 h of treatment and in granular amoebocytes even after 24 h of treatment. Thus, it seems that granular amoebocytes show different behavior depending on the exposure. The inhibition, thus, depended on both the time and exposure concentration.

3.4 Lipid peroxidation measurements

Malondialdehyde (MDA) is a lipid peroxidation subproduct. MDA production was therefore used for the evaluation of lipid peroxidation caused by CuO NPs and CuSO_4 (1, 10, and 100 $\mu\text{g mL}^{-1}$ of Cu). Significant changes in MDA production were observed in cells treated with both CuO NPs and CuSO_4 (10 and 100 $\mu\text{g mL}^{-1}$ of Cu) (Fig. 7).

The increase in MDA production was dose-dependent. The greatest MDA production was detected after cell treatment for 6 h with the greatest concentrations of CuO NPs and CuSO_4 . The MDA levels were 10 times and 13 times elevated in cells exposed to CuO NPs and CuSO_4 , respectively, (100 $\mu\text{g mL}^{-1}$ of Cu) after 6 hours of exposure (Fig. 7). MDA leakage in control samples was not observed; however, the supernatant of the treated cells contained some level of MDA (data not shown). Lipid peroxidation analyses for the 1 $\mu\text{g mL}^{-1}$ of Cu concentration (CuO NPs, CuSO_4) are not shown because the values were below the detection limit. We observed that 10 $\mu\text{g mL}^{-1}$ of Cu in the form of CuO and CuSO_4 exhibited a greater MDA concentration after 2 h of incubation with cells.

3.5 Comet assay

The DNA damage percentage (% DNA) reflects the degree of oxidative damage under some stress conditions. Comet parameters, such as % of tail DNA, olive tail, and % of head DNA, were measured to evaluate the DNA damage of coelomocytes.

The % DNA is shown as the DNA percentage in the comet tail. The % DNA in both the CuO NP and CuSO_4 treatments increased along the exposure time (Fig. 8). Significant changes in DNA damage were observed after 6 and 24 h of

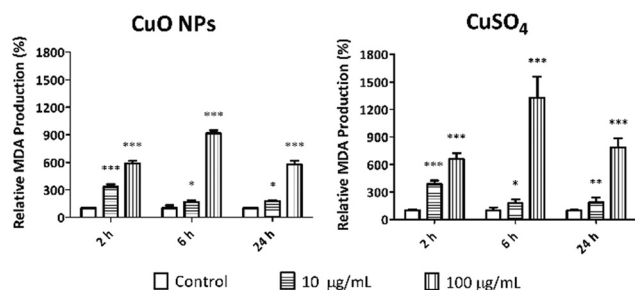


Fig. 7 MDA production in cells treated with CuO NPs and CuSO_4 . Two concentrations of CuO NPs and CuSO_4 were used (10 and 100 $\mu\text{g mL}^{-1}$ of Cu). MDA production was measured after incubation for 2, 6, and 24 h. Data are expressed as % of MDA production and as mean \pm SEM of three experiments with three replicates. *** $p < 0.001$, ** $p < 0.01$, * $p < 0.05$ according to two-way ANOVA and Bonferroni post-test.

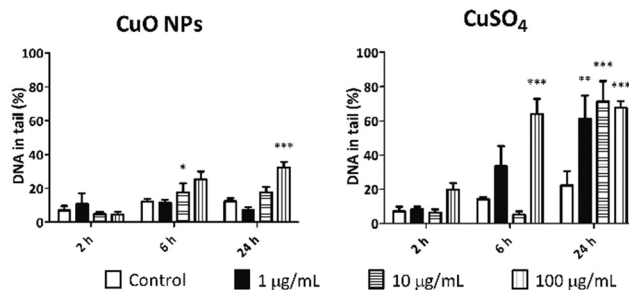


Fig. 8 Alkaline Comet assay. The % DNA in the comet tail of coelomocytes exposed to CuO NPs and CuSO_4 at 1, 10, and 100 $\mu\text{g mL}^{-1}$ of Cu after 2, 6, and 24 h of incubation. Data are expressed as a mean (%) \pm SEM of three experiments with three replicates. The means were obtained from the median of the tail % DNA of 100 comets of each replicate. *** $p < 0.001$, ** $p < 0.01$, * $p < 0.05$ according to two-way ANOVA and Bonferroni post-test.

cell incubation with CuO NPs (100 $\mu\text{g mL}^{-1}$ of Cu). Cell incubation with CuSO_4 induced even greater DNA damage compared to CuO NPs. It seems that the control effect ions (CuSO_4) have a stronger impact on cells than CuO NPs. The greatest % DNA damage was detected after incubation with 100 $\mu\text{g mL}^{-1}$ of Cu in the form of CuSO_4 for 24 h (Fig. 8).

3.6 mRNA levels of defense molecules

In addition to the cellular response, we evaluated the changes in mRNA levels of various molecules in coelomocytes after their treatment with CuO NPs and CuSO_4 (1 and 10 $\mu\text{g mL}^{-1}$ of Cu).

We screened several molecules (Tables 1 and 2) involved in various cellular functions such as metal detoxification (metallothionein), heavy metal detoxification (phytochelatin), oxidative stress (Mn-SOD, CuZn-SOD, CAT), immunity (EMAP II, fetidin, lumbricin), and signal transduction (MEK kinase 1, protein kinase C 1). Since RNA from cells exposed to the greatest concentration (100 $\mu\text{g mL}^{-1}$ of Cu) in the form of CuO NPs and CuSO_4 exhibited poor quality, most probably caused by the greater mortality of the coelomocytes, it was not used for quantitative PCR.

We observed metallothionein upregulation, which increased along the exposure time after cellular treatment with CuO NPs at both concentrations, although the greater concentration induced greater upregulation. Then, we detected catalase downregulation after 24 h (10 $\mu\text{g mL}^{-1}$ of Cu), and CuZn-SOD and Mn-SOD after 2 h (1 $\mu\text{g mL}^{-1}$ of Cu). Mn-SOD was also downregulated at the 24 h interval (1 $\mu\text{g mL}^{-1}$ of Cu). Overall, cell treatment with CuO NPs did not induce immune or signaling molecules.

In the case of cell treatment with CuSO_4 , we obtained very similar data to the case of CuO NPs. The only increased mRNA level was detected for metallothionein. Similar to CuO NPs, CuSO_4 induced downregulation in SODs and CAT, major antioxidant enzymes (Table 2). In contrast to CuO NPs, slight downregulation was also seen in signal transduction molecules. Immune defense molecules were not affected by cell treatment with CuSO_4 .

Table 1 mRNA levels of assorted molecules in coelomocytes after CuO NP treatment. mRNA changes were tested by two-way ANOVA with the Bonferroni post-test (a: $p < 0.05$, b: $p < 0.01$, c: $p < 0.001$). The control is relative to 1.00. Values < 1.00 correspond to gene downregulation, and values > 1.00 correspond to gene upregulation. Two reference genes (RPL13, RPL17) were selected as internal controls for the normalization of the other gene expression. The fold change in the mRNA level was related to the change in the settled controls. Primer sequences are shown in Table S2.† Mn-SOD: manganese superoxide dismutase; CuZn-SOD: copper–zinc-superoxide dismutase; EMAP II: endothelial monocyte-activating polypeptide-II; Fet/Lys: fetidin/lysenin; RPL 17 – ribosomal protein L17; RPL 13 – ribosomal protein L13

Function	Gene	Conc. CuO NPs ($\mu\text{g mL}^{-1}$ of Cu)	Normalized gene expression (relative to control)		
			2 h	6 h	24 h
Metal detoxification	Metallothionein	1	5.27 ± 0.88^b	2.63 ± 0.06^a	5.44 ± 0.12^b
		10	0.87 ± 0.11	1.22 ± 0.06	13.36 ± 0.35^c
Heavy metal detoxification	Phytochelatin	1	0.984 ± 0.14	0.81 ± 0.18	1.03 ± 0.16
		10	0.9 ± 0.12	1.52 ± 0.08	1.03 ± 0.15
Oxidative stress	Mn-SOD	1	0.30 ± 0.08^a	0.50 ± 0.06	0.26 ± 0.04^b
		10	0.83 ± 0.14	0.55 ± 0.12	0.46 ± 0.099
	CuZn-SOD	1	0.26 ± 0.04^c	0.95 ± 0.26	0.65 ± 0.10
		10	0.82 ± 0.12	1.04 ± 0.10	1.11 ± 0.20
		CAT	1	1.13 ± 0.15	0.55 ± 0.09
Immunity	EMAP II	10	0.84 ± 0.11	1.25 ± 0.10	0.52 ± 0.07^a
		1	0.66 ± 0.13	0.70 ± 0.09	0.91 ± 0.19
	Fetidin/lysenin	10	0.86 ± 0.11	1.38 ± 0.09	1.54 ± 0.17
		1	0.44 ± 0.06	0.77 ± 0.11	0.69 ± 0.11
		10	0.74 ± 0.10	1.51 ± 0.11	1.26 ± 0.36
Lumbricin	1	1.26 ± 0.21	0.47 ± 0.19	1.20 ± 0.31	
	10	1.03 ± 0.14	2.08 ± 0.5	0.74 ± 0.09	
	MEK kinase 1	1	0.96 ± 0.10	0.66 ± 0.07	0.69 ± 0.18
Signal transduction	MEK kinase 1	10	0.88 ± 0.12	1.49 ± 0.07	0.70 ± 0.03
		1	1.70 ± 0.28	0.64 ± 0.09	0.94 ± 0.18
	Protein kinase C 1	1	0.88 ± 0.15	1.27 ± 0.15	0.57 ± 0.18
		10			

4. Discussion

The environmental fate of some metal nanoparticles, such as CuO NPs, is currently being studied together with their

interactions with soil organisms, due to the input of 39–73% of CuO NPs and Cu NPs to landfills, and consequently to soil organisms, such as earthworms.³⁵ Therefore, since terrestrial organisms like *E. andrei* earthworms are in close contact with

Table 2 mRNA levels of assorted molecules in coelomocytes after CuSO₄ treatment. mRNA changes were tested by two-way ANOVA with the Bonferroni post-test (a: $p < 0.05$, b: $p < 0.01$, c: $p < 0.001$). The control is relative to 1.00. Values < 1.00 correspond to gene downregulation, and values > 1.00 correspond to gene upregulation. Two reference genes (RPL13, RPL17) were selected as internal controls for the normalization of the other gene expression. The mRNA fold change level was related to the change in the settled controls. Primer sequences are shown in Table S2.† Mn-SOD: manganese superoxide dismutase; CuZn-SOD: copper–zinc-superoxide dismutase; EMAP II: endothelial monocyte-activating polypeptide-II; Fet/Lys: fetidin/lysenin; RPL 17 – ribosomal protein L17; RPL 13 – ribosomal protein L13

Function	Gene	Conc. CuSO ₄ ($\mu\text{g mL}^{-1}$ of Cu)	Normalized gene expression (relative to control)		
			2 h	6 h	24 h
Metal detoxification	Metallothionein	1	0.89 ± 0.13	0.64 ± 0.17	6.93 ± 1.68^c
		10	0.97 ± 0.19	2.54 ± 0.19^c	10.44 ± 0.54^c
Heavy metal detoxification	Phytochelatin	1	1.21 ± 0.20	0.73 ± 0.33	0.8 ± 0.31
		10	0.98 ± 0.12	0.90 ± 0.06	0.88 ± 0.18
Oxidative stress	Mn-SOD	1	0.4 ± 0.07^a	0.35 ± 0.09^a	0.29 ± 0.08^a
		10	0.84 ± 0.09	0.51 ± 0.05^b	0.39 ± 0.05^c
	CuZn-SOD	1	0.29 ± 0.08^b	0.51 ± 0.12	0.82 ± 0.19
		10	0.9 ± 0.09	0.67 ± 0.03	1.07 ± 0.09
		CAT	1	0.80 ± 0.12	0.35 ± 0.08^a
Immunity	EMAP II	10	1.01 ± 0.20	0.49 ± 0.05^a	0.3 ± 0.04^b
		1	0.71 ± 0.1	0.57 ± 0.13	0.55 ± 0.3
	Fetidin/lysenin	10	0.68 ± 0.09	1.21 ± 0.08	1.71 ± 0.09^a
		1	0.78 ± 0.1	0.49 ± 0.11	0.58 ± 0.16
		10	0.58 ± 0.08	1.52 ± 0.11	0.53 ± 0.03
Lumbricin	1	1.11 ± 0.15	0.57 ± 0.15	1.18 ± 0.56	
	10	1.04 ± 0.14	1.05 ± 0.12	0.75 ± 0.06	
	MEK kinase 1	1	0.63 ± 0.08	0.44 ± 0.1^a	0.65 ± 0.15
Signal transduction	MEK kinase 1	10	0.78 ± 0.09	0.98 ± 0.23	0.88 ± 0.13
		1	0.73 ± 0.1	0.39 ± 0.09	0.69 ± 0.18
	Protein kinase C 1	10	1.06 ± 0.13	0.44 ± 0.03^b	0.29 ± 0.05^c

these NPs, better comprehension of the interaction between NPs and earthworm coelomocytes is needed.

Our findings showed that CuO NPs are located on the cell surface, and additionally are taken up by coelomocytes. Subsequently, it can lead to the activation of the earthworm immune system. To properly evaluate the NPs effects on cells, their physical and chemical characterization has to be performed. In this study, the different techniques used for the NP characterization (*i.e.* ICP-OES, TEM, MADLS, Z-potential, and UV/vis; Fig. S1 and Table S1†) showed that CuO NPs are unstable and have a tendency to aggregate.

The culture medium used for all experiments (R-RPMI 1640 medium) affects the dispersion of CuO NPs. Also, the speed of CuO NP dissolution depends on the concentration, probably due to the NP aggregation. CuO NPs interact with various ligands containing amino functional groups, such as glutamine, which results in the increased solubility of CuO NPs at neutral pH 7.4,¹¹ and in the release of Cu²⁺ ions in the cultivation medium. Furthermore, soluble copper (Cu²⁺ ions) is responsible for most of the effects derived from CuO NPs.³⁶ We suggest that NP instability and their dissolution in R-RPMI 1640 medium could be related to the presence of glutamine or other medium components and that the observed negative effects could be caused mainly by Cu²⁺ ions.

Electron microscopy revealed CuO NPs on the cell surface (Fig. 2B–D) as well as inside the cells (Fig. 3A–D). Also, clusters of CuO NPs were found over the surface and around the coelomocytes (Fig. 2B and C). The EDS analyses confirmed the copper identity of the observed objects (Fig. 2E and F). Interestingly, coelomocytes were able to engulf CuO NPs into the cytoplasm (Fig. 3); however, similar to Bigorgne *et al.*,¹⁷ NP aggregates were not found in the nucleus or mitochondria (Fig. 3A–D). The STEM/EDS-microanalysis then unequivocally confirmed copper in those aggregates (Fig. 3E–G). Internalized CuO NP clusters could act as a source of Cu²⁺ ions *in situ*, and boost cellular damage. Then, Cu²⁺ ions could oxidize the cellular membrane from the cytoplasm. This mechanism type called the “Trojan-horse” was described for human lung epithelial cells exposed to Co₃O₄ NPs,³⁷ and in earthworm coelomocytes exposed to Ag NPs.¹⁴ In both cases, the entry of NPs through the membrane is proposed, followed by the production of the negative effects caused by the NP ionic form. Thus, amoebocyte phagocytic ability could lead to NP scavenging. Therefore, this cell type can be more sensitive to NP exposure.^{14,18}

Cells treated with CuO NPs and CuSO₄ underwent apoptosis. In both populations of amoebocytes, similar apoptotic activity was detected. The effects derived from Cu²⁺ ions (CuSO₄) were displayed as the changed percentage of cells undergoing early apoptosis (Fig. 4 and 5). The percentage of cells in late apoptosis/necrosis increased following the exposure to the greatest concentration of Cu²⁺ ions, suggesting that Cu²⁺ ions are probably the principal cause. Homa *et al.* suggested that after the stimulation, cells

were less viable and they entered the apoptotic pathway. Moreover, it is worth noticing that *E. andrei* coelomocytes are rather susceptible to disintegration (necrosis). Coelomocytes can undergo programmed cell death after contact with excess bacterial or fungal products.¹⁶ Interestingly, there is an inverse correlation between antioxidant system suppression and apoptosis pathway activation.¹⁶ Our data indicate that such suppression can lead to coelomocyte disintegration instead of the apoptosis pathway.

It was described that phagocytosis is performed mainly by the amoebocyte population.^{14,17,22,38} Our results indicate that hyaline amoebocytes have a bit greater phagocytic activity than the granular amoebocytes (Fig. 6). The control untreated cells exerted rather great phagocytic activity, which is in line with the results obtained by Bigorgne *et al.* who showed that control cells without any treatment exerted around 60% phagocytic activity.³⁸ CuO NP as well as CuSO₄ cellular treatment led to decreased phagocytic activity, which is most likely due to the effect of the Cu²⁺ ions rather than the NPs themselves. In contrast with our results, Fuller-Espie and colleagues described that at lower concentrations, free radicals, phagocytosis and apoptosis are induced due to oxidative stress.³⁹ In this study, the inverse linkage of late apoptosis/necrosis with phagocytosis was observed, reflecting the impossibility of apoptotic cells engulfing beads.

Subsequently, the lipid peroxidation subproduct, a membrane permeable MDA, represents a promising biomarker of oxidative stress and oxidative cellular damage at the membrane level.⁴⁰ Our study showed significantly greater MDA production during the whole experimental period at both concentrations (10 and 100 µg mL⁻¹ of Cu) in the form of CuSO₄ and CuO NPs (Fig. 7). The possibility that Cu²⁺ ions released from NPs could undergo a Fenton-like copper redox reaction (*i.e.* copper may form the reactive hydroxyl radicals (HO[•]) in the presence of H₂O₂) cannot be excluded.¹¹ Then, HO[•] radicals can interfere with and affect the lipids.^{40–42}

Coelomocyte incubation with both CuO NPs and CuSO₄ led to nuclei DNA damage (Fig. 8), which tended to increase over time. Since CuSO₄ caused even greater DNA damage than CuO NPs, we envisage the involvement of Cu²⁺ rather than the NPs themselves. Thus, the exposure to soluble Cu (Cu²⁺ ions) from CuSO₄ is more toxic than the same Cu²⁺ ion amount in CuO NPs, as it has also been shown in trout erythrocytes exposed to both of them.⁴³ MDA interaction with nucleosides leading to the formation of MDA-DNA adducts is proposed, as was previously suggested by Ayala and colleagues.⁴⁰ This study shows that lipid peroxidation may occur and may induce DNA damage.

Further, expression changes of several immune-related genes and genes involved in oxidative stress and signal transduction in CuO NPs and CuSO₄-treated coelomocytes were assessed. Nanoparticles were described to alter the expression of some genes involved in oxidative stress regulation and immune signaling.^{15,23} Two genes encoding important molecules involved in protection against oxidative

stress, catalase and manganese superoxide dismutase (Mn-SOD), were downregulated. Similarly, catalase was downregulated in earthworm coelomocytes exposed to silver NPs.¹⁴ Mn-SOD and catalase are antioxidant enzymes that protect biological macromolecules against oxidative damage. They were previously described to be upregulated upon oxidative stress caused by assorted pollutants in earthworms to maintain their homeostasis.^{44,45} Mincarelli *et al.* described that copper excess did not trigger the earthworm antioxidant enzyme response.⁴⁶ Interestingly, the inactivated antioxidant¹⁶ system can push coelomocytes to undergo apoptosis or necrosis. However, it was suggested that SOD activity is not a suitable biomarker for oxidative stress induced by heavy metals, as it exerts a great variability of responses.^{45,47} Qi *et al.* described that catalase is less sensitive but more effective than SOD at eliminating ROS in earthworms.⁴⁴ As mentioned previously, potentially, H₂O₂ can be degraded in the presence of copper released from CuO NPs upon a Fenton-like copper redox reaction, which may result in catalase downregulation. As a response of cell exposure to CuO NPs at both concentrations utilized (1 and 10 µg mL⁻¹ of Cu), metallothionein (MT) expression significantly increased over time in agreement with other studies.⁴⁶ Metallothioneins represent cysteine-rich proteins playing a dual role as early defense molecules against toxic metal ions and oxidative stress.⁴⁸ MEK kinase 1 was previously shown to play a role in stress-signal transduction and induction of MT expression in human⁴⁹ and murine cells,⁵⁰ but not in earthworm coelomocytes.¹⁴ Similarly, we did not detect any significant upregulation of this gene in *E. andrei*. Some studies have suggested that earthworms possess a strong tolerance to metals, most probably due to increased MT levels after the metal exposure.^{14,51}

Conclusions

Our study shows that the impact of CuO NPs on earthworm immunocompetent cells was mainly due to solubilized Cu²⁺ ions rather than the NPs themselves. We observed decreased cell viability, together with decreased phagocytic activity of amoebocytes as a consequence of CuO NP and CuSO₄ treatment. We did not observe increased transcript levels of genes involved in the protection against oxidative stress, catalase, and Mn-SOD, indicating that the antioxidative system was not initiated, or it was promptly switched off. In contrast, metallothionein expression, which protects cells against toxic metal ions, was significantly increased. We also detected increased malondialdehyde concentrations, a lipid peroxidation subproduct, which was most probably responsible for DNA damage and subsequent cell death.

Moreover, transmission, scanning electron microscopy, and X-ray microanalysis (TEM, SEM and EDS) provided data concerning CuO NP distribution in coelomocytes. Analyses confirmed that their cell surface was in contact with CuO NPs, and that CuO NPs were taken up by coelomocytes. Determining the parameters related to oxidative stress,

immune reactivity and genotoxicity provided valuable data for further assessment of NP impact on soil organisms.

Funding

This project received funding from the European Union's Horizon 2020 research and innovation programme under the Marie Skłodowska-Curie grant agreement No. 67188. This work was supported by Grant QK1910095 of the Ministry of Agriculture of the Czech Republic and by the Center for Geosphere Dynamics (UNCE/SCI/006). The Core Facility for Electron Microscopy CF, IMG AS CR is supported by the Czech-BioImaging large RI project (LM2018129 funded by MEYS CR) and by the European Regional Development Fund – Project “Modernization and support of research activities of the national infrastructure for biological and medical imaging Czech-BioImaging” (No. CZ.02.1.01/0.0/0.0/16_013/0001775).

Author contributions

Conceptualization: N. I. N. P., P. P.; data curation: N. I. N. P., R. R., J. D., J. S., P. P.; formal analysis: N. I. N. P., R. R., J. S., M. P.; funding acquisition: O. B., D. P., M. P., T. C., P. P.; investigation: R. R., J. D.; methodology: N. I. N. P., J. S., P. P.; project administration: R. R., T. C., M. B., P. P.; resources: O. B., M. P.; software: N. I. N. P., J. D., O. B.; supervision: J. D., J. S., P. P.; validation: O. B., O. K., M. B., P. P.; visualization: N. I. N. P., J. D., O. B., D. P.; writing – original draft: N. I. N. P., writing – review and editing: R. R., O. B., J. S., T. C., P. P.

Conflicts of interest

The authors declare that the research was conducted in the absence of commercial or financial relationships that could lead to a potential conflict of interest.

Acknowledgements

The authors acknowledge the Cytometry and Microscopy Facility at the Institute of Microbiology of the ASCR, v.v.i. for the support of the staff and the use of their equipment, Martí Busquets Fité (Applied Nanoparticles SL) for his support on nanoparticle characterization, and we acknowledge support of CMS-Biocev Biophysical techniques (LM2015043 funded by MEYS CR). The authors gratefully acknowledge access to the electron microscopy facility, supported by project LO1509 of the Ministry of Education, Youth and Sports of the Czech Republic.

Notes and references

- 1 D. Gharailou, *A review of market studies in different fields of nanotechnology*, StatNano Publications, 2018.
- 2 V. Rajput, T. Minkina, B. Ahmed, S. Sushkova, R. Singh, M. Soldatov, B. Laratte, A. Fedorenko, S. Mandzhieva, E. Blicharska, J. Musarrat, Q. Saquib, J. Flieger and A.

- Gorovtsov, *Rev. Environ. Contam. Toxicol.*, 2020, **252**, 51–96.
- 3 E. Swart, J. Dvorak, S. Hernadi, T. Goodall, P. Kille, D. Spurgeon, C. Svendsen and P. Prochazkova, *Nanomaterials*, 2020, **10**(7), 1337.
 - 4 D. Boraschi, A. Alijagic, M. Auguste, F. Barbero, E. Ferrari, S. Hernadi, C. Mayall, S. Michelini, N. I. Navarro Pacheco, A. Prinelli, E. Swart, B. J. Swartzwelter, N. G. Bastus, L. Canesi, D. Drobne, A. Duschl, M. A. Ewart, J. Horejs-Hoeck, P. Italiani, B. Kemmerling, P. Kille, P. Prochazkova, V. F. Puentes, D. J. Spurgeon, C. Svendsen, C. J. Wilde and A. Pinsino, *Small*, 2020, **16**, e2000598.
 - 5 S. Henriksson, F. Bjurlid, A. Rotander, M. Engwall, G. Lindstrom, H. Westberg and J. Hagberg, *Sci. Total Environ.*, 2017, **580**, 564–571.
 - 6 C. D. Rich, A. C. Blaine, L. Hundal and C. P. Higgins, *Environ. Sci. Technol.*, 2015, **49**, 881–888.
 - 7 J. Kilpi-Koski, O. P. Penttinen, A. O. Vaisanen and C. A. M. van Gestel, *Environ. Sci. Pollut. Res.*, 2019, **26**, 15095–15104.
 - 8 J. G. Coleman, D. R. Johnson, J. K. Stanley, A. J. Bednar, C. A. Weiss, Jr., R. E. Boyd and J. A. Steevens, *Environ. Toxicol. Chem.*, 2010, **29**, 1575–1580.
 - 9 J. M. Unrine, S. E. Hunyadi, O. V. Tsyusko, W. Rao, W. A. Shoultz-Wilson and P. M. Bertsch, *Environ. Sci. Technol.*, 2010, **44**, 8308–8313.
 - 10 A. A. Keller, A. S. Adeleye, J. R. Conwas, K. L. Garner, L. Zhao, G. N. Cherr, J. Hong, J. L. Gardea-Torresdey, H. A. Godwin, S. Hanna, Z. Ji, C. Kaweeteerawat, S. Lin, H. S. Lenihan, R. J. Miller, A. E. Nel, J. R. Peralta-Video, S. L. Walker, A. A. Taylor, C. Torres-Duarte, J. I. Zink and N. Zuverza-Mena, *NanoImpact*, 2017, **7**, 28–40.
 - 11 Z. Wang, A. von dem Bussche, P. K. Kabadi, A. B. Kane and R. H. Hurt, *ACS Nano*, 2013, **7**, 8715–8727.
 - 12 P. Sima, in *Immunology of Annelids*, ed. V. Vetvicka, P. Sima, E. L. Cooper, M. Bilej and P. Roch, CRS Press, Boca Raton, Ann Arbor, London, Tokyo, 1994, pp. 11–165.
 - 13 P. Engelmann, Y. Hayashi, K. Bodo, D. Ernszt, I. Somogyi, A. Steib, J. Orban, E. Pollak, M. Nyitrai, P. Nemeth and L. Molnar, *Dev. Comp. Immunol.*, 2016, **65**, 41–52.
 - 14 Y. Hayashi, P. Engelmann, R. Foldbjerg, M. Szabo, I. Somogyi, E. Pollak, L. Molnar, H. Autrup, D. S. Sutherland, J. Scott-Fordsmand and L. H. Heckmann, *Environ. Sci. Technol.*, 2012, **46**, 4166–4173.
 - 15 Y. Hayashi, T. Miclaus, P. Engelmann, H. Autrup, D. S. Sutherland and J. J. Scott-Fordsmand, *Nanotoxicology*, 2016, **10**, 303–311.
 - 16 J. Homa, M. Stalmach, G. Wilczek and E. Kolaczowska, *J. Comp. Physiol., B*, 2016, **186**, 417–430.
 - 17 E. Bigorgne, L. Foucaud, C. Caillet, L. Giamberini, J. Nahmani, F. Thomas and F. Rodius, *J. Nanopart. Res.*, 2012, **14**(7), 959.
 - 18 S. Gupta, T. Kushwah and S. Yadav, *Nanoscale Res. Lett.*, 2014, **9**, 259.
 - 19 S. Carbone, T. Hertel-Aas, E. J. Joner and D. H. Oughton, *Chemosphere*, 2016, **162**, 16–22.
 - 20 M. Li, Y. Yang, J. Xie, G. Xu and Y. Yu, *Sci. Total Environ.*, 2019, **687**, 71–76.
 - 21 A. Romero-Freire, S. Lofts, F. J. Martin Peinado and C. A. M. van Gestel, *Environ. Toxicol. Chem.*, 2017, **36**, 137–146.
 - 22 N. I. Navarro Pacheco, R. Roubalova, J. Semerad, A. Grasserova, O. Benada, O. Kofronova, T. Cajthaml, J. Dvorak, M. Bilej and P. Prochazkova, *Nanomaterials*, 2021, **11**, 250.
 - 23 S. P. Curieses, N. Garcia-Velasco, E. Urionabarrenetxea, M. E. Sáenz, E. Bilbao, W. D. Di Marzio and M. Soto, *Ecotoxicol. Environ. Saf.*, 2017, **141**, 57–63.
 - 24 K. Tatsi, B. J. Shaw, T. H. Hutchinson and R. D. Handy, *Ecotoxicol. Environ. Saf.*, 2018, **166**, 462–473.
 - 25 A. Gautam, A. Ray, S. Mukherjee, S. Das, K. Pal, S. Das, P. Karmakar, M. Ray and S. Ray, *Ecotoxicol. Environ. Saf.*, 2018, **148**, 620–631.
 - 26 Y. Hayashi, T. Miclaus, C. Scavenius, K. Kwiatkowska, A. Sobota, P. Engelmann, J. J. Scott-Fordsmand, J. J. Enghild and D. S. Sutherland, *Environ. Sci. Technol.*, 2013, **47**, 14367–14375.
 - 27 I. Mullerova, *Scanning*, 2001, **23**, 379–394.
 - 28 G. S. Reynolds, *Science*, 1963, **139**, 383–389.
 - 29 O. Benada and V. Pokorny, *J. Electron Microsc. Tech.*, 1990, **16**, 235–239.
 - 30 M. Vippola, M. Valkonen, E. Sarlin, M. Honkanen and H. Huttunen, *Nanoscale Res. Lett.*, 2016, **11**, 169.
 - 31 N. W. M. Ritchie, J. Davis and D. E. Newbury, *Microsc. Microanal.*, 2008, **14**(Suppl 2), 1176–1177.
 - 32 J. Semerad, M. Cvancarova, J. Filip, J. Kaslik, J. Zlota, J. Soukupova and T. Cajthaml, *Chemosphere*, 2018, **213**, 568–577.
 - 33 I. H. Cigerci, M. M. Ali, S. Y. Kaygisiz and R. Liman, *Chemosphere*, 2016, **144**, 754–757.
 - 34 P. L. Olive and J. P. Banath, *Nat. Protoc.*, 2006, **1**, 23–29.
 - 35 A. Caballero-Guzman and B. Nowack, *J. Cleaner Prod.*, 2018, **203**, 990–1002.
 - 36 H. Zhang, Z. Ji, T. Xia, H. Meng, C. Low-Kam, R. Liu, S. Pokhrel, S. Lin, X. Wang, X. Liao, M. Wang, L. Li, R. Rallo, R. Damoiseaux, D. Telesca, L. Madler, Y. Cohen, J. Zink and A. Nel, *ACS Nano*, 2012, **6**, 4349–4368.
 - 37 L. K. Limbach, P. Wick, P. Manser, R. N. Grass, A. Bruinink and W. J. Stark, *Environ. Sci. Technol.*, 2007, **41**, 4158–4163.
 - 38 E. Bigorgne, L. Foucaud, E. Lapied, J. Labille, C. Botta, C. Sirguy, J. Falla, J. Rose, E. J. Joner, F. Rodius and J. Nahmani, *Environ. Pollut.*, 2011, **159**, 2698–2705.
 - 39 S. L. Fuller-Espie, F. M. Bearoff and M. A. Minutillo, *Pedobiologia*, 2011, **54**, S31–S36.
 - 40 A. Ayala, M. F. Munoz and S. Arguelles, *Oxid. Med. Cell. Longevity*, 2014, **2014**, 360438.
 - 41 A. N. Pham, G. Xing, C. J. Miller and T. D. Waite, *J. Catal.*, 2013, **301**, 54–64.
 - 42 J. Semerad, M. Moeder, J. Filip, M. Pivokonsky, A. Filipova and T. Cajthaml, *Environ. Sci. Pollut. Res.*, 2019, **26**(32), 33670–33682.
 - 43 G. Isani, M. L. Falcioni, G. Barucca, D. Sekar, G. Andreani, E. Carpena and G. Falcioni, *Ecotoxicol. Environ. Saf.*, 2013, **97**, 40–46.
 - 44 S. Qi, D. Wang, L. Zhu, M. Teng, C. Wang, X. Xue and L. Wu, *Environ. Sci. Pollut. Res.*, 2018, **25**, 14138–14147.

- 45 R. Roubalova, J. Dvorak, P. Prochazkova, F. Skanta, N. I. Navarro Pacheco, J. Semerad, T. Cajthaml and M. Bilej, *Ecotoxicol. Environ. Saf.*, 2018, **159**, 363–371.
- 46 L. Mincarelli, L. Tiano, J. Craft, F. Marcheggiani and C. Vischetti, *Ecotoxicology*, 2019, **28**(8), 938–948.
- 47 T. G. Honsi, L. Hoel and J. V. Stenersen, *Pedobiologia*, 1999, **43**, 652–657.
- 48 F. Reinecke, O. Levanets, Y. Olivier, R. Louw, B. Semete, A. Grobler, J. Hidalgo, J. Smeitink, A. Olckers and F. H. Van der Westhuizen, *Biochem. J.*, 2006, **395**, 405–415.
- 49 E. Hyun-Jeong and C. Jinhee, *Environ. Sci. Technol.*, 2010, **44**, 8337–8342.
- 50 Y. H. Hsin, C. F. Chen, S. Huang, T. S. Shih, P. S. Lai and P. J. Chueh, *Toxicol. Lett.*, 2008, **179**, 130–139.
- 51 S. Ecimovic, M. Velki, R. Vukovic, I. Stofa Camagajevac, A. Petek, R. Bosnjakovic, M. Grgic, P. Engelmann, K. Bodo, V. Filipovic-Marijic, D. Ivankovic, M. Erk, T. Mijosek and Z. Loncaric, *Chemosphere*, 2018, **212**, 307–318.